AIMETA 2017
XXIII Conference
The Italian Association of Theoretical and Applied Mechanics
Luigi Ascione, Valentino Berardi, Luciano Feo, Fernando Fraternali and Antonio Michele Tralli (eds.)
Salerno, Italy, 4–7 September 2017

DOMAIN EVOLUTION IN FERROELECTRIC THIN FILMS: A PHASE-FIELD APPROACH

P. Fedeli[1] **and A. Frangi**[1]

[1]Department of Civil and Environmental Engineering, Politecnico di Milano
Piazza Leonardo da Vinci 32, 20133 Milan, Italy
e-mail: patrick.fedeli@polimi.it, attilio.frangi@polimi.it

Keywords: phase-field; ferroelectrics; domain evolution; grain orientation.

Abstract. *We implement a phase field method for the analysis of ferroelectric thin films with the aim of investigating the effect of grain orientation. We present some benchmarks with literature examples and finally discuss a preliminary investigation of a multigrain structure highlighting its impact on the size and shape of the hysteresis cycle.*

1 INTRODUCTION

Ferroelectric thin films find nowadays an increasing number of applications in microsystems, such as actuators, sensors and storage devices [1], since they exhibit a strong electromechanical coupling (piezoelectricity). Prominent materials for piezoelectric applications are $PbTiO_3$ and $Pb(Zr,TI)O_3$, which are typically processed in the form of polycrystals.

In what follows the material will be partitioned in *grains* each having a specific homogeneous crystallographic orientation. Below the Curie temperature, each grain presents a spontaneous electrical polarization which can be however reoriented by applying an external electrical or stress field. The regions with uniform polarization within one grain are called ferroelectric *domains*, and the interface boundary between two adjacent domains is called *domain wall*. The polarization evolution within one domain, domain-wall motions and grain orientation strongly affect the macroscopic properties of ferroelectrics. Being able to model the evolution of domains and of polarization is key to many practical applications such as the simulation of the hysteresis loop between the average polarization and the applied electric field.

A critical literature review of the different methods available has been presented in [2]. However, the phase field approach has recently emerged as the preferred tool [3]-[7]. This method is based on the Landau-Devonshire theory of ferroelectrics [8]-[9], in which a form for free energy density is postulated and the domain evolution is simulated without introducing any a priori assumption.

The paper is organized as follows. In Section 2 we rapidly review the phase field formulation, while Section 3 is devoted to its finite element implementation. Some literature benchmarks are presented in Sections 4.1-4.2. Finally, an application of the model to investigate the effects of grain orientation in ferroelectric polycrystals is proposed in Section 4.3.

2 PHASE FIELD MODEL

We introduce the governing equations for the phase field method adopted, while a more exhaustive treatment can be found e.g. in [4]-[7].

Mechanical equilibrium is imposed in Ω, in the presence of body forces F_i and tractions t_i on the surface Γ_t:

$$\begin{aligned} \sigma_{ij,j} + F_i = 0 \quad &\text{in} \quad \Omega \\ \sigma_{ij}\, n_j = t_i \quad &\text{on} \quad \Gamma_t \end{aligned} \tag{1}$$

where σ_{ij} are the components of the Cauchy stress tensor. The electric field vector E_i and the electric displacement vector D_i are governed by the quasi-static Maxwell equations

$$\begin{aligned} D_{i,i} = q \quad &\text{in} \quad \Omega \\ D_i\, n_i + \omega = 0 \quad &\text{in} \quad \Gamma_\omega \\ E_i = -\frac{\partial \varphi}{\partial x_i} \quad &\text{in} \quad \Omega \\ \varphi = \bar{\varphi} \quad &\text{on} \quad \Gamma_\phi \end{aligned} \tag{2}$$

in which φ is the scalar electric potential, q and ω are the volume and surface charge density and $\bar{\varphi}$ is the potential imposed on the electrodes. Finally, we assume the validity of the generalized form of the Ginzburg-Landau equation describing the evolution process of the material polarization P_i:

$$\beta_{ij} \frac{\partial P_j}{\partial t} = \left(\frac{\partial \psi}{\partial P_{i,j}} \right)_{,j} - \frac{\partial \psi}{\partial P_i} \tag{3}$$

where $\psi = \psi(P_i, P_{i,j}, \varepsilon_{ij}, D_i)$ is the free energy density and β_{ij} is the inverse mobility tensor. The free energy density for a single grain is taken as a polynomial function:

$$\begin{aligned}\psi =& \alpha_i P_i^2 + \alpha_{ij} P_i^2 P_j^2 + \alpha_{ijk} P_i^2 P_j^2 P_k^2 + \frac{1}{2} g_{ijkl} P_{i,j} P_{k,l} \\ &+ \frac{1}{2} c_{ijkl} (\varepsilon_{ij} - \varepsilon_{ij}^s)(\varepsilon_{kl} - \varepsilon_{kl}^s) + \frac{1}{2\kappa_0} (D_i - P_i)(D_i - P_i)\end{aligned} \tag{4}$$

The first three terms denote the Landau energy density, which describes a non-convex function with minima at the spontaneous polarization states. The fourth one penalizes large variations of the polarization and governs the formation and evolution of domain walls. The other two terms represent the mechanical and electrical contributions, respectively. Elastic strains are expressed as the difference between the linearized total strains ε_{ij} and the inelastic strains ε_{ij}^s, expressed in terms of the polarization as $\varepsilon_{ij}^s = Q_{ij} P_i P_j$, where Q_{ij} are the electrostrictive coefficients. The constant κ_0 represents the vacuum permittivity. A more detailed description of the free energy for $PbTiO_3$ is discussed in [4],[7] and [10].

Given the assumed form of the free energy, the constitutive laws flow as follows:

$$\begin{aligned}\sigma_{ij}(\varepsilon_{ij}, P_i) &= \frac{\partial \psi}{\partial \varepsilon_{ij}} \\ D_i &= \kappa_0 E_i + P_i\end{aligned} \tag{5}$$

3 FINITE ELEMENT IMPLEMENTATION

The governing equations of the phase-field model formulated in the previous section are first imposed in weak form introducing suitable test fields:

$$\int_\Omega \sigma_{ij}\, \varepsilon_{ij}(\tilde{u}_i)\, \mathrm{d}\Omega - \int_\Omega F_i \tilde{u}_i\, \mathrm{d}\Omega - \int_{\Gamma_t} t_i\, \tilde{u}_i\, \mathrm{d}\Gamma = 0 \qquad \forall \tilde{u}_i \in \mathcal{C}(0) \tag{6}$$

$$\int_\Omega D_i \frac{\partial \tilde{\varphi}}{\partial x_i}\, \mathrm{d}\Omega - \int_\Omega q \tilde{\varphi}\, \mathrm{d}\Omega - \int_{\Gamma_\omega} \omega\, \tilde{\varphi}\, \mathrm{d}\Gamma = 0 \qquad \forall \tilde{\varphi} \in \mathcal{C}(0) \tag{7}$$

$$\int_\Omega \left[\frac{\partial \psi}{\partial P_{i,j}} \tilde{P}_{i,j} + \frac{\partial \psi}{\partial P_i} \tilde{P}_i + \beta_{ij} \frac{\partial P}{\partial t} \tilde{P}_i \right] \mathrm{d}\Omega = 0 \qquad \forall \tilde{P}_i \in \mathcal{C}(0) \tag{8}$$

In the present investigation we restrict ourselves to 2D problems in which the polarization and the electric field have only in-plane components, and furthermore we assume a generalized plane strain condition:

$$P_3 = 0 \qquad E_3 = 0 \qquad \varepsilon_{13} = \varepsilon_{23} = 0,\ \varepsilon_{33} = \varepsilon_\perp$$

where $\varepsilon_\perp$ is the normal spontaneous strain. The domain S is partitioned in grains (see e.g. Figure 3) and every grain is meshed with six-node triangles. In each element the fields are interpolated using suitable shape functions:

$$\{u_h\} = [N_u]\,\{U_e\} \qquad \varphi_h = [N_\varphi]\,\{\varphi_e\} \qquad \{P_h\} = [N_P]\,\{P_e\} \tag{9}$$

Quadratic shape functions are chosen for the displacement and electric potential, whereas the polarization has a linear interpolation. Following standard differentiation procedures, the strain vector, the electric field and the polarization gradient can also be expressed in terms of elemental nodal values:

$$\{\varepsilon_h\} = [B_u]\,\{U_e\} \qquad \{E_h\} = -[B_\varphi]\,\{\varphi_e\} \qquad \{\nabla P_h\} = [B_P]\,\{P_e\} \tag{10}$$

Collecting all the unknowns in the arrays $\{\mathbb{U}\}, \{\Phi\}, \{\mathbb{P}\}$ and taking into account the constitutive relationships, the discretized weak form generates a system of non-linear equations:

$$[\mathbb{K}_{\mathrm{U}}]\{\mathbb{U}\} + [\hat{\mathbb{K}}_{\mathrm{UP}}]\{\mathbb{P}\} = \{\mathbb{F}_{\mathrm{U}}\} \tag{11}$$

$$[\mathbb{K}_{\varphi}]\{\Phi\} + [\mathbb{K}_{\varphi\mathrm{P}}]\{\mathbb{P}\} = \{\mathbb{F}_{\varphi}\} \tag{12}$$

$$[\mathbb{M}]\{\dot{\mathbb{P}}\} + ([\mathbb{K}_{\mathrm{G}}] + [\hat{\mathbb{K}}_{\mathrm{P}}])\{\mathbb{P}\} + [\hat{\mathbb{K}}_{\mathrm{PU}}]\{\mathbb{U}\} + [\mathbb{K}_{\mathrm{P}\varphi}]\{\Phi\} = \{0\} \tag{13}$$

Several methods are available for the approximate solution in time of the system. They are based on a subdivision of the time interval $[0, T]$ in N time steps Δt such that $T = N\Delta t$. In this work we adopt a simple semi-implicit (staggered) approach.

Eqs. (11)-(12) are imposed at time t_{n+1} and are solved explicitly using the polarization computed at iteration n:

$$[\mathbb{K}_{\mathrm{U}}]\{\mathbb{U}_{n+1}\} = \{\mathbb{F}_{\mathrm{U}}\} - [\hat{\mathbb{K}}_{\mathrm{UP}}]\{\mathbb{P}_n\} \tag{14}$$

$$[\mathbb{K}_{\varphi}]\{\Phi_{n+1}\} = \{\mathbb{F}_{\varphi}\} - [\mathbb{K}_{\varphi\mathrm{P}}]\{\mathbb{P}_n\} \tag{15}$$

The time derivative of polarization vector is approximated by backward finite differences:

$$\{\dot{\mathbb{P}}\} = \frac{\{\mathbb{P}_{n+1} - \mathbb{P}_n\}}{\Delta t} \tag{16}$$

so that eq.13 becomes:

$$\begin{aligned} \frac{[\mathbb{M}]}{\Delta t}\{\mathbb{P}_{n+1} - \mathbb{P}_n\} + ([\mathbb{K}_{\mathrm{G}}] + [\hat{\mathbb{K}}_{\mathrm{P}}])\{\mathbb{P}_{n+1}\} \\ + [\hat{\mathbb{K}}_{\mathrm{PU}}]\{\mathbb{U}_{n+1}\} + [\mathbb{K}_{\mathrm{P}\varphi}]\{\Phi_{n+1}\} = \{0\} \end{aligned} \tag{17}$$

in which $\{\mathbb{U}_{n+1}\}$ and $\{\Phi_{n+1}\}$ are known. The non-linear system eq.(17) is solved iteratively applying a Newton-Raphson scheme. The residuum $\{\mathbb{R}\}$ at iteration k is

$$\{\mathbb{R}(\{\mathbb{P}^{[k]}\})\} = \left(\frac{[\mathbb{M}]}{\Delta t} + [\mathbb{K}_{\mathrm{G}}] + [\hat{\mathbb{K}}_{\mathrm{U}}]\right)\{\mathbb{P}^{[k]}\} + [\hat{\mathbb{K}}_{\mathrm{PU}}]\{\mathbb{U}_{n+1}\} - \frac{[\mathbb{M}]}{\Delta t}\{\mathbb{P}_n\} + [\mathbb{K}_{\mathrm{P}\varphi}]\{\Phi_{n+1}\} \tag{18}$$

and is expanded to first-order at the previous iterate:

$$\{\mathbb{R}^{[k+1]}\} \simeq \{\mathbb{R}^{[k]}\} + [\nabla_{\mathbb{P}}\{\mathbb{R}\}](\{\mathbb{P}^{[k]}\})\{\delta\mathbb{P}^{[k]}\} \tag{19}$$

where

$$[\nabla_{\mathbb{P}}\{\mathbb{R}\}] = \left(\frac{[\mathbb{M}]}{\Delta t} + [\mathbb{K}_{\mathrm{G}}]\right) + [\nabla_{\mathbb{P}}([\hat{\mathbb{K}}_{\mathrm{P}}]\{\mathbb{P}\} + [\hat{\mathbb{K}}_{\mathrm{PU}}]\{\mathbb{U}_{n+1}\})] \tag{20}$$

is the tangent stiffness matrix.

4 NUMERICAL SIMULATIONS

4.1 Single grain with domain wall motions

In order to assess the capabilities of our method, we initially present some benchmarks with examples taken from [11]. In particular, the movement of domain walls is investigated in homogeneous specimens made of lead titanate ($PbTiO_3$). The material coefficients utilized are listed in Table 1. In all simulations, traction free and charge free boundary conditions are assumed

Coefficient	Value	Unit		Coefficient	Value	Unit
α_1	-0.1725	(aJ)(nm)/(aC)$^{-2}$				
α_{11}	-0.073	(aJ)(nm)^5/(aC)$^{-4}$		C_{11}	174	(aJ)/(nm)^3
α_{12}	0.26	(aJ)(nm)^5/(aC)$^{-4}$		C_{12}	79	(aJ)/(nm)^3
α_{111}	0.61	(aJ)(nm)^9/(aC)$^{-6}$		C_{44}	111	(aJ)/(nm)^3
α_{112}	0.75	(aJ)(nm)^9/(aC)$^{-6}$				
G_{11}	0.2768	(aJ)(nm)^3/(aC)$^{-2}$		Q_{11}	0.089	(nm)^4/(aC)$^{-2}$
G_{12}	0	(aJ)(nm)^3/(aC)$^{-2}$		Q_{12}	-0.026	(nm)^4/(aC)$^{-2}$
G_{44}	0.1384	(aJ)(nm)^3/(aC)$^{-2}$		Q_{44}	0.0338	(nm)^4/(aC)$^{-2}$

Table 1: Values of material coefficients for $PbTiO_3$ [12].

and the electric field is applied imposing different electric potential values on the boundaries, simulating the presence of electrodes.

Let us first consider a rectangular specimen made of a single grain, with length 20 nm and height 5 nm. The domain is discretized as shown in Fig. 1 with approximately 1400 triangular elements. The pictures on the left refer to the case where the electrodes cover the whole bottom and top borders, with the imposed potential indicated. The electric field (see Fig. 1-a) is vertical. Fig. 1-b, presents the selected initial configuration with two domains separated by a single 180° interface. The domain-wall moves to the right subjected to the imposed electric field, as illustrated in Fig. 1-c, and the domain on the right eventually vanishes.

The pictures on the right, on the contrary, refer to the case where electrodes cover only a portion of the top and bottom borders, while an additional one is position on the right border. In this case the 90° interface stabilizes when it reaches the end of the electrodes.

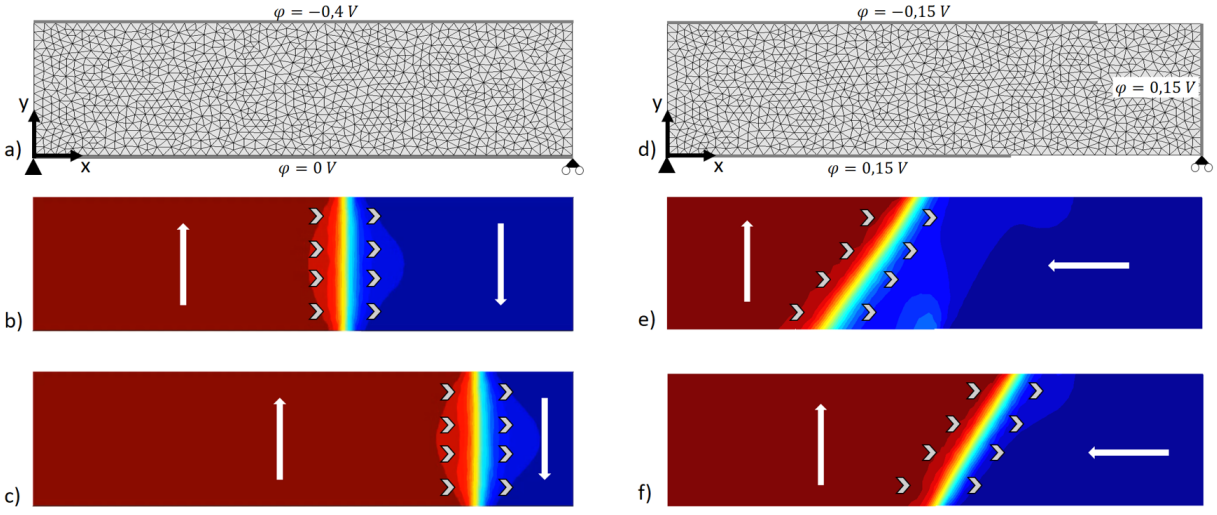

Figure 1: Vertical polarization distribution. a) - d) Finite element setup for 180°/90° domain wall motions; b) - e) initial configuration; c) - f) domain wall movement. The arrows indicate orientation of polarization vectors.

4.2 Single grain with holes

Let us consider a single grain of dimensions 10x10 nm, with a square opening of 5x5 nm in the middle. As shown in Fig. 2-a, potential boundary conditions are imposed on the top and

bottom lines. The domain structure in Fig. 2-b is obtained when $\lambda/10$ is equal to coercive field intensity $E_c = 0.13$ V/nm. The presence of the hole affects the ferroelectric domain distribution, resulting in a multi-domain configuration. Applying an electric field in the negative y-direction, the domains evolve and the stable pattern of Fig. 2-c is obtained.

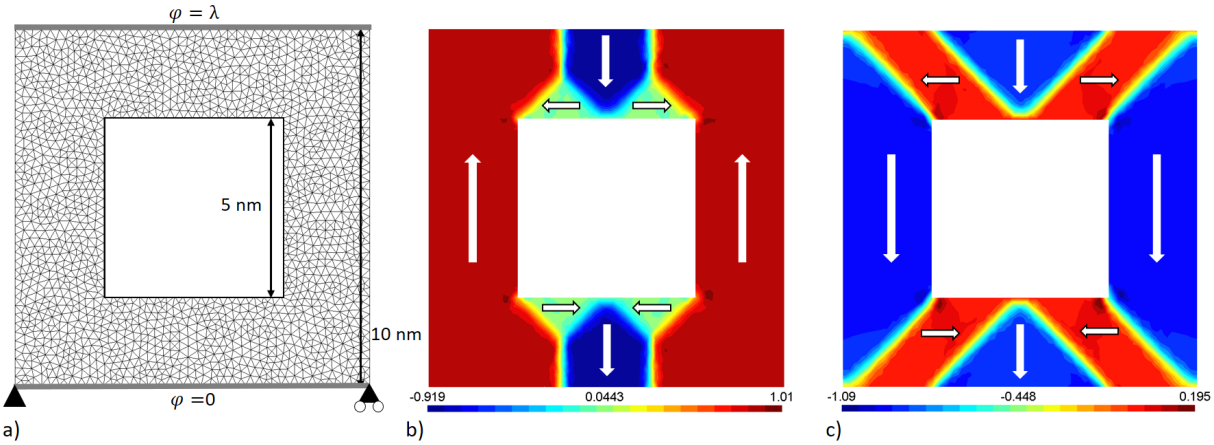

Figure 2: Vertical polarization distribution. a) Finite element setup; b) domain configuration after an initial poling with $\lambda/10 = E_c$; c) final configuration with $\lambda/10 = -0.6E_c$ (E_c is the electric coercive field). The arrows indicate orientation of polarization vectors.

4.3 Multigrain structure and hysteresis loop

Most ferroelectrics are polycrystals composed of several grains having different orientations, which influence the polarization distribution in the domains.

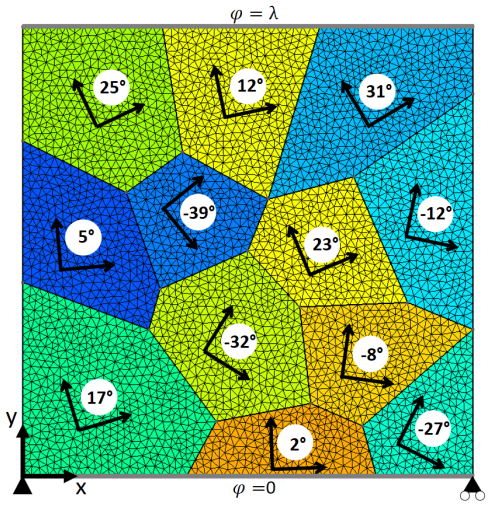

Figure 3: Finite element discretization for polycrystal composed of several grains. The crystallographic orientations are assigned randomly in the range $\pm 40°$ with respect to the reference axis.

In this Section we analyse the configuration depicted in Figure 3, where the square specimen of size 20x20 nm contains 12 grains. We aim at showing how the multigrain nature of piezo films can impact on their properties, and in primis on the hysteresis loop.

The energy density introduced in Section 2 has been defined for a single grain. In the presence of multiple grains with orientations described in 2D by an angle θ, the free energy is

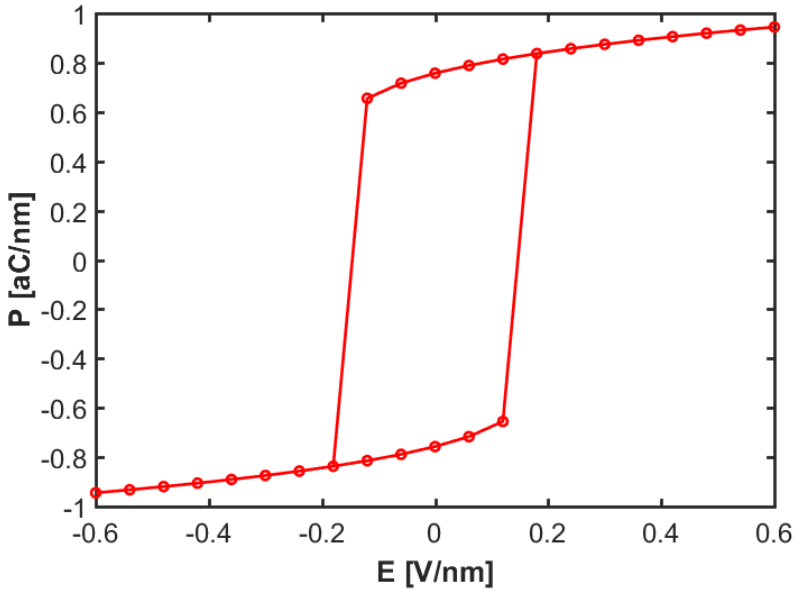

Figure 4: Hysteresis loop for a single grain, perfectly oriented in the vertical direction.

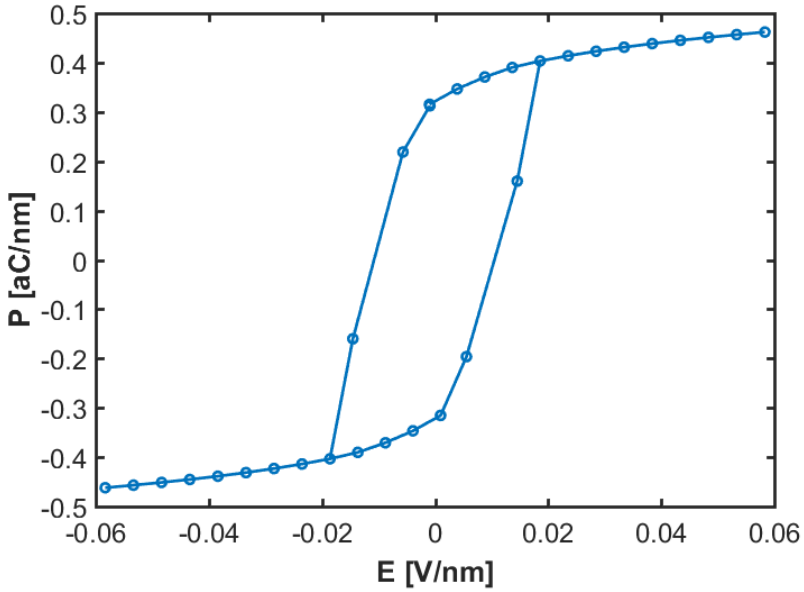

Figure 5: Hysteresis loop in the multigrain case. The crystallographic orientations are assigned randomly in the range $\pm 40^\circ$ with respect to the reference axis.

expressed in the local reference system of each grain while the polarization, the strain and the electric field E_i are backrotated to the global system by means of standard rotation matrices: $P_i = R_{ij}P_j^G$, $\varepsilon_{ij} = R_{ki}R_{lj}\varepsilon_{kl}^G$ and $E_i = R_{ij}E_j^G$, in which the superscript G denotes the global fields and R_{ij} is the rotation matrix [13].

Two electrodes are placed on the bottom and top borders, as in the first example of Section 4.1. In order to evaluate only the effects of grain orientations, we consider grain boundaries of zero thickness, imposing the zero polarization. A cyclic history of electric field is applied in the vertical by varying the value of λ.

Figures 4-5 present the hysteresis loops obtained for a homogeneous material and the multigrain specimen on Figure 3 respectively. Macroscopic values are obtained by averaging polarizations over the entire simulated domain. The remnant polarization and the coercive field in the polycrystal with different grain orientations are considerably smaller than those in the homogeneous crystal.

REFERENCES

[1] P. Muralt, Ferroelectric thin films for micro-sensors and actuators: a review, *J. Micromech. Microeng.*, **10**, 136–146, 2000

[2] D. Fang, F. Li, B. Liu, Y. Zhang, J. Hong, X. Guo, Advances in developing electromechanically coupled computational methods for piezoelectrics/ferroelectrics at multiscale, *Applied Mechanics Reviews*, **65**, 1–52, 2013

[3] L.-Q. Chen, Phase-field models for microstructure evolution, *Annu Rev Mater Res* **32**, 113–140, 2002

[4] J. Wang, S.-Q. Shi, L.-Q. Chen, Y. Li, T.-Y. Zhang, Phase field simulations of ferroelectric/ferroelastic polarization switching, *Acta Materialia*, **52**, 749-764, 2004

[5] Y. Su , C.M. Landis, Continuum thermodynamics of ferroelectric domain evolution: theory, finite element implementation, and application to domain wall pinning, *J Mesh Phys Solids* **55**, 280–305, 2007

[6] A. Kontsos, C.M. Landis, Phase-Field modeling of domain structure energetics and evolution in ferroelectric thin films, *Journal of Applied Mechanics* **77**, 1–12, 2010

[7] J. Wang, M. Kamlah, Three-dimensional finite element modeling of polarization switching in a ferroelectric single domain with an impermeable notch, *Smart Mater. Struct.* **18**, 1–7, 2009

[8] A. Devonshire *Theory of ferroelectrics, Vol 10, 3th Edition*. Philipp Mag, 1954

[9] M.E. Gurtin, Generalized Ginzburg-Landau and Cahn-Hilliard equations based on a microforce balance, *Phys D*, **92**, 178–192, 1996

[10] B. Völker, P. Marton, P. Elsässer, M. Kamlah, Multiscale modeling for ferroelectric materials: a transition form the atomic level to phase-field modeling, *Continuum Mech. Thermodyn.*, **23**, 435–451, 2011

[11] M. Krauß, I. Münch, A selective enhanced FE-method for phase field modeling of ferroelectric materials, *Comput. Mech*, **57**, 105–122, 2016

[12] M.J. Haun, E. Furman, S.J. Jang, H. A. McKinstry, L. E. Cross, Thermodynamic theory of PbTiO2, *J. Appl. Phys.*, **62(8)**, 3331-3338, 1987

[13] J. Wang, W. Shu, T. Shimada, T. Kitamura, T.-Y. Zhang, Role of grain orientation distribution in the ferroelectric and ferroelastic domain switching of ferroelectric polycrystals, *Acta Materialia*, **52**, 749-764, 2004